forests

MDPI

Article

Experimental Study of Beam Stability Factor of Sawn Lumber Subjected to Concentrated Bending Loads at Several Points

Effendi Tri Bahtiar [1,2,*], Erizal Erizal [3], Dede Hermawan [1], Naresworo Nugroho [1] and Rizky Hidayatullah [1]

[1] Forest Products Department, Faculty of Forestry and Environment, IPB University (Bogor Agricultural University), Kampus IPB Dramaga, Bogor 16153, Indonesia
[2] Civil Engineering Study Program, Faculty of Engineering, Pakuan University, Bogor 16129, Indonesia
[3] Civil and Environment Engineering Department, Faculty of Agricultural Technology, IPB University (Bogor Agricultural University), Kampus IPB Dramaga, Bogor 16153, Indonesia
* Correspondence: bahtiar_et@apps.ipb.ac.id or bahtiar_et@yahoo.com

Abstract: The beam stability factor (C_L) is applied in construction practices to adjust the reference bending design value (F_b) of sawn lumber to consider the lateral-torsional buckling. Bending tests were carried out on 272 specimens of four wood species, namely, red meranti (*Shorea* sp.), mahogany (*Swietenia* sp.), pine (*Pinus* sp.), and agathis (*Agathis* sp.), to analyze a simply supported beam subjected to concentrated loads at several points. The empirical C_L value is a ratio of the modulus of rupture (S_R) of a specimen to the average S_R of the standard-size specimens. The non-linear regression estimated the Euler buckling coefficient for sawn lumber beam (K_{bE}) in this study as 0.413, with 5% lower and 5% upper values of 0.338 and 0.488. Applying the 2.74 factor, which represents an approximately 5% lower exclusion value on the pure bending modulus of elasticity (E_{min}) and a factor of safety, the adjusted Euler buckling coefficient (K_{bE}') value for a timber beam was 1.13 (0.92–1.34), which is within the range approved by the NDS (K_{bE}' = 1.20). This study harmonizes the NDS design practices of C_L computation with the empirical results. Because agathis has the lowest ductility (μ), most natural defects (smallest strength ratio, S), and highest E/S_R ratio, the agathis beam did not twist during the bending test; instead, it failed before twisting could occur, indicating inelastic material failure. Meanwhile the other specimens (pinus, mahogany, and red meranti), which have smaller E/S_R ratio, higher ductility, and less natural defects, tended to fail because of lesser beam stability. This phenomenon resulted in the C_L curve of agathis being the highest among the others. The C_L value is mathematically related to the beam slenderness ratio (R_B) and the E/S_R ratio. Because the strength ratio (S) and ductility ratio (μ) have significant inverse correlations with the E/S_R ratio, they are correlated with the C_L value. Applying the C_L value to adjust the characteristic bending strength is safe and reliable, as less than 5% of the specimens' S_R data points lie below the curve of the adjusted characteristics values.

Keywords: beam stability factor; characteristics values; engineering structures; lateral-torsional buckling; mechanical properties; stability experiment; timber construction

check for updates

Citation: Bahtiar, E.T.; Erizal, E.; Hermawan, D.; Nugroho, N.; Hidayatullah, R. Experimental Study of Beam Stability Factor of Sawn Lumber Subjected to Concentrated Bending Loads at Several Points. *Forests* **2022**, *13*, 1480. https://doi.org/10.3390/f13091480

Academic Editor: Barbara Ozarska

Received: 18 August 2022
Accepted: 11 September 2022
Published: 14 September 2022

Publisher's Note: MDPI stays neutral with regard to jurisdictional claims in published maps and institutional affiliations.

Copyright: © 2022 by the authors. Licensee MDPI, Basel, Switzerland. This article is an open access article distributed under the terms and conditions of the Creative Commons Attribution (CC BY) license (https://creativecommons.org/licenses/by/4.0/).

1. Introduction

Timbers are often used as structural components such as beams, columns, and trusses in residential housing [1], multi-story buildings [2], cooling towers [3–5], and bridges [6]. Beam design involves analyzing member strength, stability, and stiffness for four essential criteria (e.g., bending (including stability), deflection, horizontal shear, and bearing). In addition to mechanical resistance and serviceability, a designer must verify other requirements (e.g., environmental condition, durability aspects, fire resistance, and fatigue) to build a timber construction. Timber beam strength is commonly determined through edgewise bending tests with the loads applied to the narrow face [7,8]. Edgewise bending stiffness and strength are the essential grade-determining properties (GDP) in wood strength

grading, and can be predicted by the flatwise modulus of elasticity [9]. Timber grading machines based on edgewise bending excitation are available in the European market; however, their applications are limited [10] because a greater applied load is needed to bend timber edgewise than flatwise.

Columns and beams can be categorized as short, intermediate, and long according to the slenderness ratio (λ) and beam slenderness ratio (R_B), respectively. A rectangular cross-sectional wooden column is long if the ratio of the length to the least cross-sectional dimension (L/h) range is 27–50, following the Rankine–Gordon formula [11], while a round bamboo culm beam is long if the slenderness ratio (λ) is more than 30.5 for Guadua [12] and 32 for *G. apus* [13], following the Ylinen formula. While buckling does not occur in a short beam or column [14,15] it usually does for intermediate or long ones. A beam slenderness ratio (R_B) less than 11 indicates a short beam, while an R_B range of 11–50 indicates intermediate and long beams [16].

A slender beam tends to buckle and torsion, which is known as lateral–torsional buckling. Lateral–torsional buckling occurs on fixed [17], cantilevered [18], and a single-span beams [19]. Beams with square cross-sections are not susceptible to lateral–torsional buckling. ASTM D143 [20] designates the square cross-section bending test specimen ($5 \times 5 \times 76$ cm^3 primary method and $2.5 \times 2.5 \times 41$ cm^3 secondary method); thus, many researchers [4,5,12,21–23] have chosen it as a standard specimen in bending tests. Following the British Standard [24], static bending tests are carried out on $2 \times 2 \times 30$ cm^3 dimension specimens as well [22,25]. Lateral–torsional buckling does not occur for circular cross-section beams [26], hollow circular cross-sectional beams (e.g., plumbing [27], bamboo [28–30]), or box beams [31]. Lateral–torsional buckling occurs when a slender beam is subjected to bending loads; deformation occurs until it reaches its critical load [32], then the beam deflects out-of-plane accompanied by twisting. Beam deformation includes in-plane deformation, out-of-plane deformation, and twisting [33], all of which are involved when lateral–torsional buckling occurs. Lateral supports need to be applied to limit these deformations and ensure beam stability. Beams with sufficient lateral support are not susceptible to lateral–torsional buckling. Suryoatmono and Tjondro studied the lateral–torsional buckling of a rectangular beam loaded by a concentrated load [34]. The beam was laterally supported at both ends, and the results showed that the beam reached its critical load without rotating.

Lateral buckling may occur on slender beams, and can govern beam failure; thus, lateral support must be provided to prevent rotation when the depth of the long bending member exceeds its width ($d > b$) [35]. The beam stability factor (C_L) is applied to adjust the reference bending design value of timber structure components subjected to bending [33,35,36] in order to consider the effect of lateral–torsional buckling.

The distance between lateral support points along the beam length, termed the unsupported length (l_u), affects the beam stability factor (C_L). The unsupported length l_u is converted into the effective span length (l_e) following the beam loading configuration. The beam slenderness ratio (R_B), which is calculated following Equation (1), is the basis for stability design in beams. The allowable bending stress ($F_b{}'$) in beams is specified based on the beam slenderness ratio for the three ranges: short beams ($R_B \leq 10$), intermediate beams ($11 < R_B \leq C_k$), and long beams ($C_k < R_B \leq 50$). The beam stability factor (C_L) formulas were derived by Zahn [37] for three separate ranges (Equations (2–4)) and adopted by the National Design Specification (NDS) 1986 [38]. In the equation, F_b' is the allowable bending stress, E is the modulus of elasticity, and R_B is the beam slenderness ratio. The transition point of the beam slenderness ratio between intermediate and long beams (C_k) is calculated following Equation (5). Zhan [39] reevaluated the NDS 1986 [38] C_L formula by deriving an elastic buckling criterion for simply supported beams under any combination of strong-axis bending loads, weak-axis bending loads, axial compression, equal end couples, and water ponding to account for the interaction between bending moment and axial compression.

NDS has adopted a single continuous C_L formula (Equation (6)) since 1991, which applies to all range of beam slenderness ratio (R_B) and replaces Equations (2)–(4) for

determining the effects of beam slenderness ratio on allowable bending design values (F_b). The Euler buckling coefficient for a beam (K_{bE}) in the NDS 1991 [40] was 0.438, replacing the value of 1.44/3.3 in Equation (4). The design formula (Equation (6)) was proposed by Zahn [41], which simplified the Ylinen column buckling formula by setting its non-linear parameter for beam (c) equal to 0.95. This C_L formula (Equation (6)) is more accurate and general for beam slenderness ratios less than 50 ($R_B < 50$) and is designated in the current NDS. The Indonesian National Standard (SNI) 7973:2013 [33], which recently adopted the NDS 2012 [35], proposes this C_L formula as well. The F_{bE} factor in Equation (6) is the critical buckling design value, which is calculated following Equation (7).

$$R_B = \sqrt{\frac{l_e d}{b^2}} \tag{1}$$

$$F_b' = F_b, \text{ for short beam } (R_B \leq 10) \tag{2}$$

$$F_b' = F_b\left[1 - \frac{1}{3}\left(\frac{R_B}{C_k}\right)^4\right], \text{ for intermediate beam } (11 < R_B \leq C_k) \tag{3}$$

$$F_b' = \frac{1.44E}{3.3(R_B)^2}, \text{ for long beam } (C_k < R_B \leq 50) \tag{4}$$

$$C_k = 0.811\sqrt{\frac{E}{F_b}} \tag{5}$$

$$C_L = \frac{1+\left(\frac{F_{bE}}{F_b^*}\right)}{1.9} - \sqrt{\left[\frac{1+\left(\frac{F_{bE}}{F_b^*}\right)}{1.9}\right]^2 - \frac{\left(\frac{F_{bE}}{F_b^*}\right)}{0.95}}, \text{ for } (R_B \leq 50) \tag{6}$$

$$F_{bE} = \frac{K_{bE}\, E}{R_B{}^2} = \frac{0.438E}{R_B{}^2} \tag{7}$$

After 1997, the NDS has chosen to report E_{min} rather than E; thus, the K_{bE} value of 0.438 is replaced with 1.20 of the adjusted Euler buckling coefficient ($K_{bE}{}'$) (Equation (8)) to correspond to the factor of 2.74. The factor of 2.74 represents a 5% lower exclusion value of the modulus of elasticity (E_{min}) (1.03 times tabulated E values) and a safety factor of 1.66 [16]. The F_{bE} calculation by $K_{bE}{}'$ and E_{min} follows Equation (8). The SNI 7973:2013 [33] and the current NDS currently designate this value.

$$F_{bE} = \frac{K_{bE}'\, E_{\min}}{R_B{}^2} = \frac{1.20E_{\min}}{R_B{}^2} \tag{8}$$

Several reports on timber beam stability subjected to bending are available in the literature. Hindman et al. [18] studied lateral–torsional buckling on rectangular cantilever beams to validate the C_L formula and reported that the C_L formula was non-conservative for Laminated Veneer Lumber (LVL), although it was suitable for solid sawn lumber. Kimble and Bender [42] studied the stability of built-up timber beams with various E values in which the beam has a slenderness ratio value of 26.20 (unbraced long beams); their results showed that the obtained C_L value was low. Du et al. [43,44] reported that the deck-board stiffness significantly affected the lateral–torsional buckling capacity of twin-beam deck systems. Hu et al. [45,46] developed an energy-based solution to analyze the lateral–torsional buckling of a wooden beam with a midspan lateral brace and indicated that such beams were prone to symmetric and antisymmetric mode buckling patterns. St-Amour and Doudak [47] conducted a sensitivity analysis on a wood I-joist and determined that the critical buckling load is affected by the longitudinal modulus of elasticity, the transverse shear modulus of the flanges, and the elastic modulus of the web. They determined that the equivalent moment factor theory is more adaptable than the Euler elastic buckling theory to predict the I-joist's critical buckling moment [48]. Sahraei et al. [49] proposed

a simplified expression to account for moment gradient, load height, and pre-buckling deformation effects for elastic lateral–torsional buckling of wooden beams.

The available standards designate various methods for designing a beam able to resist lateral–torsional buckling, however, these approaches are significantly different and lack consistency [50]. Balaz [51] proposed formulas to harmonize the different rules in the Eurocode concerning critical moments and suggested replacing the warping constant of a solid rectangular cross-section beam. AFPA [52] described the basis of the current effective length approach used in the NDS and summarized the equivalent uniform moment factor approach, providing a comparison between the two approaches and proposing modifications to the NDS design provisions. The present study aims to analyze the response of beams made from several locally available commercial lumber varieties subjected to concentrated loads at several points in order to validate the beam stability factor (C_L) formula designated by NDS 2012 [35], which has been adopted by SNI 7973:2013 [33]. Because red meranti, mahogany, pinus, and agathis sawn lumber are abundantly available in the building material market and are commonly used for structural construction members, they were chosen as the specimens in this study. Center point loading bending tests of small clear specimens and several point loading bending tests of full-sized specimens were conducted to measure the empirical beam stability factor ($C_{L,e}$), then the non-linear regression was employed to estimate the K_{bE} value. The empirical C_L values, estimated best-fit curve, and 5% upper and 5% lower curves were plotted in Cartesian Diagrams together with the building code's designated graph to justify the harmony of the empirical and designated C_L values.

2. Materials and Methods

2.1. Specimen Preparation

The materials were 272 pieces of specimens consisting of 200 small pieces (2.5 × 2.5 × 41) cm^3 and 72 full-size pieces (4 × 10 × 130) cm^3. The specimens were sawn lumber of red meranti (*Shorea* sp.), mahogany (*Swietenia* sp.), pine (*Pinus* sp.), and agathis (*Agathis* sp.) purchased from commercial timber markets in Bogor, West Java–Indonesia. All specimens were air-dried in indoor environmental conditions (27 °C and 80% RH) for a month to reach equilibrium moisture content. All experimental work was undertaken in the Wood Engineering Laboratory, Faculty of Forestry and Environment, IPB University (Bogor, Indonesia).

2.2. Small Specimen Bending Test

The small specimens of red meranti, mahogany, pine, and agathis, 50 pieces each, were prepared for the bending test. The length (L), width (b), and depth (d) of each specimen were measured employing a digital caliper with an accuracy of 0.01 mm. The masses were measured three times: before the bending test (m_0), after the bending test (m_1), and after oven-drying (m_{ot}). The oven-drying was carried out at (103 ± 2) °C for two days to evaporate water content in the specimens. Moisture content measurements were conducted soon after the bending test. The moisture content (M_c) was calculated following Equation (9).

$$M_c = \frac{m_1 - m_{ot}}{m_{ot}} 100\% \quad (9)$$

The static bending test was carried out following the ASTM D143 secondary method [20] (Figure 1). The span of the specimen was 360 mm in order to maintain a span-to-depth ratio of 14. The specimens were then bending tested with center-point loading using a five-ton capacity Instron type 3369 Universal Testing Machine (UTM). Both supports were rollers with 2 cm diameter. The load was applied continuously throughout the test at the movable crosshead motion rate of 1.3 mm/min. The modulus of elasticity (E) and modulus

of rupture (S_R) values were calculated following Equations (10) and (11). The E values were calculated within the proportional region of the load–deflection curve.

$$E = \frac{PL^3}{4\Delta bd^3} \tag{10}$$

$$S_R = \frac{3P_{max}L}{2bd^2} \tag{11}$$



Figure 1. Static bending test of small specimens following the ASTM D143 secondary method [20]. The specimen size was 25 × 25 × 410 mm with the span length of 360 mm and loading speed of 1.3 mm/min.

The small specimens' E and S_R statistics data, including the mean, standard deviation (s), minimum value, maximum value, and coefficient of variance (CV), were summarized. The 5% exclusion limit ($R_{0.05}$) values of E and S_R were calculated to determine the bending strength characteristic value (R_k) following ASTM D2915 [53] and D5457 [54]. Normal, lognormal, and Weibull standard distributions were applied to fit the experimental data, and the best choice was determined through the Anderson-Darling test [8,12,13].

Material ductility may affect the beam stability. Ductility is a structure's ability to undergo significant deformation in the plastic ranges before its collapse [55], which is often expressed as the ratio between ultimate displacement (Δ_u) and yield displacement (Δ_y) (Equation (12)) [55]. Muñoz et al. [56] stated the ultimate and yield displacement ratio in Equation (12) as the ductility ratio (μ), while Jorissen and Fragiacomo [57] termed it the ductility factor. Ultimate displacement (Δ_u) is the displacement at the ultimate load (F_u), while yield displacement (Δ_y) can be calculated following several methods suggested by researchers [58–60] and standard specifications [61–63]. The yield displacement (Δ_y) in this study is equal to deformation at $0.5F_u$ following Karacabeyli and Ceccotti [58].

$$\mu = \frac{\Delta_u}{\Delta_y} \tag{12}$$

2.3. Full-Size Specimen Bending Test

Full-size specimens of red meranti, mahogany, pine, and agathis, 18 pieces each, were prepared. Every sawn lumber piece was visually graded following ASTM D245 [64] (Figure 2). Defects and imperfections in the wood were identified and measured. Three indicating defects were observed, namely, the slope of the grain, knot diameter, and the presence of shakes, checks, and splits, then converted into strength ratio (S) values.

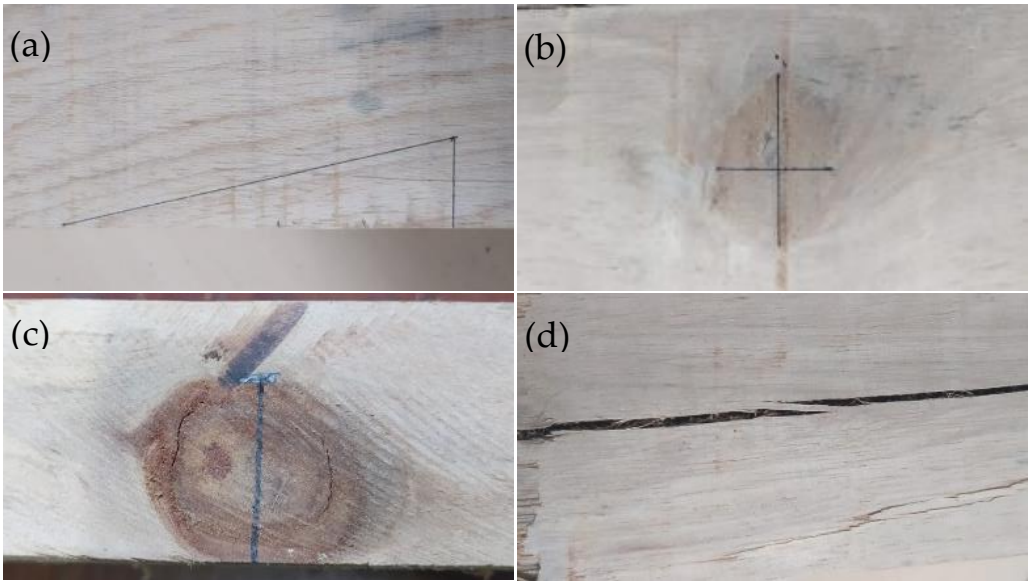


Figure 2. Measurement of defects and imperfections to calculate the strength ratio value (S) of bending following ASTM D245 [64]: (**a**) the slope of the grain was measured by the tangent of the angle between the direction of the fibers and the edge of the specimen; (**b**) knots at the wide face were measured by the average of their largest and smallest diameter; (**c**) knots at the narrow face were measured by their width between the lines enclosing the knot and parallel to the edges of the specimen; and (**d**) shakes, checks, and splits were measured at the ends of the specimen.

The length (L) of each specimen was measured employing a tape measure, while width (b) and depth (d) were measured using a digital caliper with an accuracy of 0.01 mm. The mass was measured three times: before the bending test (m_0), after the bending test (m_1), and after oven-drying (m_{ot}). The specimens used for measuring m_1 and m_{ot} were $4 \times 4 \times 4$ cm^3 and were cut near the bending test specimen's failure position. The M_c value was calculated according to Equation (9). The density (ρ) was calculated in air-dry conditions before the bending test of a full-size specimen (Equation (13)), while the relative density or specific gravity (G_b) was calculated according to Equation (14).

$$\rho = \frac{m_0}{L \times b \times h} \tag{13}$$

$$G_b = \frac{\rho}{(1 + M_c)\rho_{\text{water}}} \tag{14}$$

The values of E and S_R in the edgewise configuration bending tests were determined employing UTM SATEC/Baldwin. The span of the bending test was 120 cm. The specimens were tested in simply-supported bending with various concentrated loading configurations, namely, center point loading, third point loading, fourth point loading, fifth point loading, and sixth point loading (Figure 3). Lateral supports were applied at every point of loading. Figure 3 shows the position of the five linear variable displacement transducers (LVDTs) which were employed to measure the deflection. As a control, bending tests with a center-point loading configuration and without lateral support were carried out. The formulae of E and S_R with various loading configurations are summarized in Table 1.

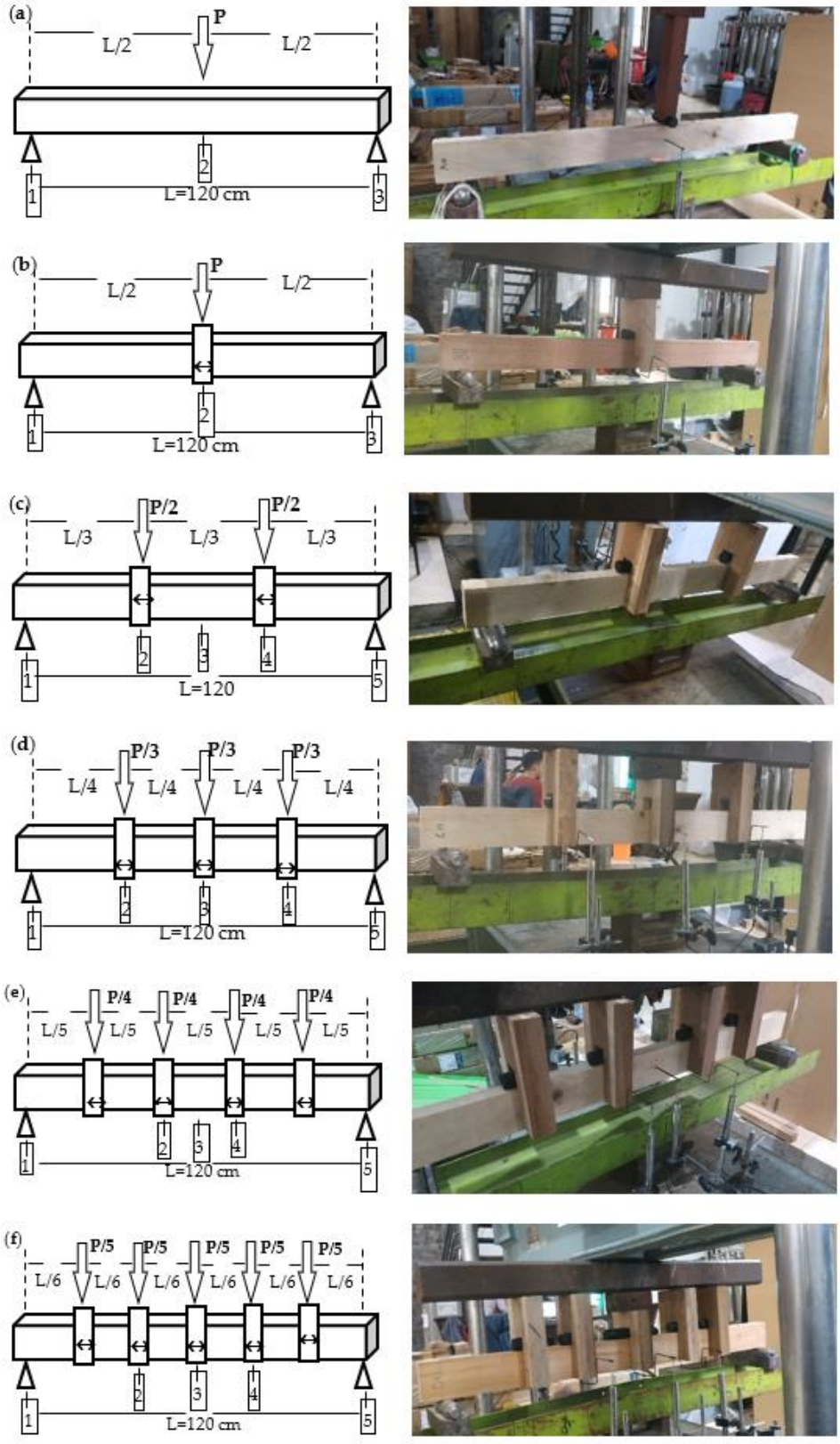


Figure 3. Scheme of a single-span beam subjected to concentrated loads at several points: (**a**) center-point loading without lateral support, (**b**) center-point loading, (**c**) third point loading, (**d**) fourth point loading, (**e**) fifth point loading, (**f**) sixth point loading (Note: P = applied load; L = span; ↔ = lateral support; ⇕ = LVDT).

Table 1. The simply supported beam bending formula.

Loading Configuration	Bending Formula	
center-point loading with or without lateral support	$E = \frac{PL^3}{4\Delta bd^3}$	$S_R = \frac{3P_{max}L}{2bd^2}$
third point loading with lateral supports	$E = \frac{23PL^3}{108\Delta bd^3}$	$S_R = \frac{P_{max}L}{bd^2}$
fourth point loading with lateral supports	$E = \frac{19PL^3}{96\Delta bd^3}$	$S_R = \frac{P_{max}L}{bd^2}$
fifth point loading with lateral supports	$E = \frac{9PL^3}{50\Delta bd^3}$	$S_R = \frac{9P_{max}L}{10bd^2}$
sixth point loading with lateral supports	$E = \frac{11PL^3}{60\Delta bd^3}$	$S_R = \frac{9P_{max}L}{10bd^2}$

Note: P_{max} = maximum load borne by beam or column loaded to failure (N), P = increment of applied load below the proportional limit (N), L = span of a beam (mm), Δ = increment of deflection of beam's neutral axis measured at midspan over distance L and corresponding load P (mm), b = width of beam (mm), d = depth of beam (mm).

2.4. Beam Stability Factor (C_L) Value Calculation

The effective span length (l_e) of the beams was determined following Table 2. The beam slenderness ratio (R_B) of each specimen was calculated (Equation (1)), while the critical buckling design value of a beam (F_{bE}) was calculated per Equation (7). The empirical C_L ($C_{L,e}$) values from the experimental study were calculated per Equation (15). S_{Ri} is the modulus of rupture (MOR) value of each specimen. $\overline{S_R}$ is the average MOR value of the small-size specimen (b = d = 2.5 cm), tested in bending at a standardized condition following ASTM D143 secondary methods [20].

$$C_{L,e} = S_{Ri} \,/\, \overline{S_R} \tag{15}$$

Table 2. Effective span length (l_e) for bending members.

No	Single Span Beam	Effective Span Length (l_e)	
		$l_u/d < 7$	$l_u/d \geq 7$
1.	center-point loading without lateral support	$l_e = 1.8\ l_u$	$l_e = 1.37\ l_u + 3d$
2.	center-point loading with lateral support	$l_e = 1.11\ l_u$	
3.	third point loading with lateral supports	$l_e = 1.68\ l_u$	
4.	fourth point loading with lateral supports	$l_e = 1.54\ l_u$	
5.	fifth point loading with lateral supports	$l_e = 1.68\ l_u$	
6.	sixth point loading with lateral supports	$l_e = 1.73\ l_u$	

Note: l_e is effective span length for bending members (mm), l_u is the distance between such points of intermediate lateral support (mm).

The non-linear regression model was derived from Equation (6), with F_{bE} substituted by Equation (7), and is presented in Equation (16). Then the non-linear parameter for beam (c) was set to 0.95, E was the small specimens' average modulus of elasticity, F_b was the experimental value of $\overline{S_R}$, and the K_{bE} value was estimated by the regression coefficient (a) (Equation (17)). The non-linear regression analysis with Levenberg–Marquardt algorithm iteration [65] was applied to estimate the empirical value of K_{bE} from experimental results. The starting value of the iteration was 0.438, following Zahn [41].

$$C_L = \frac{\left[1 + K_{bE}\frac{E}{F_b R_B{}^2}\right]}{2c} - \sqrt{\left[\frac{1 + K_{bE}\frac{E}{F_b R_B{}^2}}{2c}\right]^2 - \frac{K_{bE}\frac{E}{F_b R_B{}^2}}{c}} \tag{16}$$

$$\hat{y} = \frac{(1+ax)}{2c} - \sqrt{\left(\frac{1+ax}{2c}\right)^2 - \frac{ax}{c}} \tag{17}$$

where $\hat{y}$ is the estimated empirical C_L obtained through experimental study ($C_{L,e}$), x is $E/(\overline{S_R} \times R_B{}^2)$, c is set to 0.95, and a is the regression coefficient. The regression coefficient (a) estimates the Euler buckling coefficient (K_{bE}).

3. Results and Discussion

3.1. Moisture Content (M_c), Density (ρ), and Specific Gravity (G_b)

Many physical and mechanical properties of wood depend upon its moisture content. The specimens' average moisture content ranged from 13.45% to 16.98% (Figure 4a), the common air-dry moisture content in Bogor, West Java Indonesia [13,14,66–68]. The specimens' moisture content is within the permissible range in the Indonesian Wooden Building Code (PKKI) regulation [69], which states that the average air-dry moisture content is 15% and its range is 12–18%. The wood density (ρ) depends on its moisture content because both the mass and volume of wood depend upon it. The density of air-dry wood varies significantly between species. The wood relative density or specific gravity (G_b) in this study was referenced based on air-dry volume and oven-dry mass. The average results of ρ and G_b measured in this experimental study are presented in Figure 4, and conform to the ρ value stated in PKKI [69].

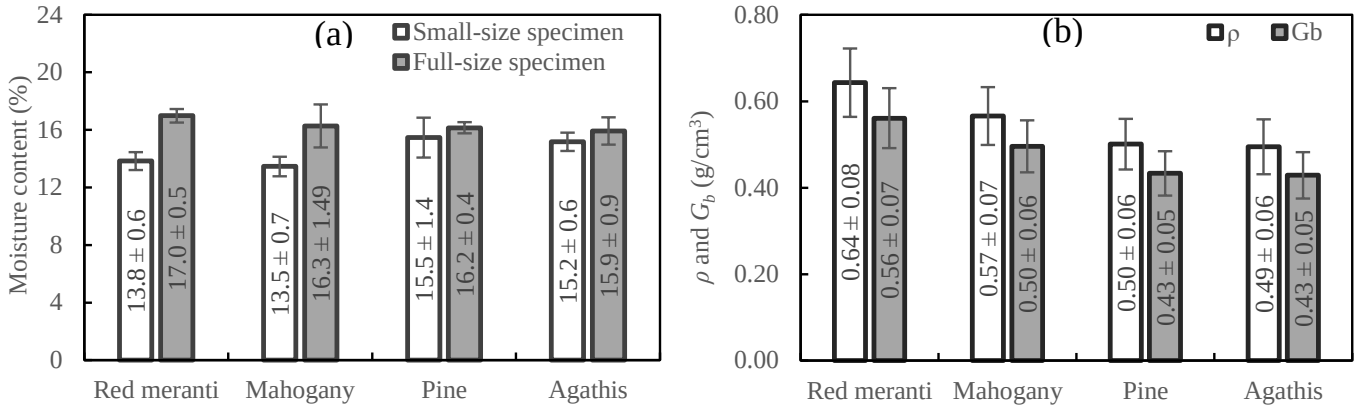


Figure 4. (**a**) Air-dry moisture content (M_c); (**b**) density (ρ) and specific gravity (G_b).

3.2. Flexural Properties of the Small Specimens

The average modulus of elasticity (E) and modulus of rupture (MOR, S_R) values of the small specimens of red meranti, mahogany, pine, and agathis are summarized in Table 3; they were similar to previous reports [70–73]. Based on their respective E values, red meranti is graded in the E16–E27 strength class, mahogany is E10–E20 strength class, pine is E6–E21 strength class, and agathis is E12–E17 strength class, per SNI 7973:2013 [33]. Similar to Firmanti et al. report on tropical timber [8], the Weibull distribution was the best fit among others for most of the experimental data. The ASTM D5457 [54] standard distribution for wood strength is assumed to be the Weibull distribution, while European countries commonly designate a log-normal distribution. In this study, the Anderson–Darling tests evaluated the goodness of fit of experimental data (modulus of elasticity (E) and modulus of rupture (S_R)), and the best-fit distribution was chosen among three standard distribution (Weibull, lognormal, and normal) (Table 4). The characteristic bending values (E_{min} and F_b) were determined by estimating their 5% exclusion limits. The 5% exclusion limits ($R_{0.05}$) of E and S_R are presented in Table 4, with the best-fit values were shown in bold font.

Table 3. The small specimens' flexural properties.

		Modulus of Elasticity (E, MPa)					**Modulus of Rupture (S_R, MPa)**					
	n	**Min**	**Max**	**Mean**	***s***	**CV (%)**	**Min**	**Max**	**Mean**	***s***	**CV (%)**	$\frac{E}{S_R}$
Red meranti	50	8346	13879	11001	1379	12.54	44.07	90.87	72.42	12.15	16.77	151.91
Mahogany	50	5275	10393	8033	1079	13.43	38.83	94.69	70.47	11.37	16.14	113.99
Pine	50	3460	10695	7218	1837	25.45	28.87	76.87	55.15	10.18	18.46	130.88
Agathis	50	6020	8604	6976	618	8.85	17.71	25.03	20.59	1.58	7.67	336.21

Table 4. The estimated population parameter of the small specimens' flexural properties.

Timber Species	Red Meranti		Mahogany		Pine		Agathis	
Parameter	***E***	***S_R***	***E***	***S_R***	***E***	***S_R***	***E***	***S_R***
Weibull	AD = 0.467 p = 0.244	AD = 0.291 p > 0.250	AD = 0.256 p > 0.250	AD = 0.544 p = 0.172	AD = 0.191 p > 0.250	AD = 0.476 p > 0.250	AD = 1.675 p < 0.010	AD = 2.561 p < 0.010
5% PE	**8346**	**48.37**	**5949**	**48.56**	3936	**35.60**	5784	17.44
Lognormal	AD = 0.916 p = 0.018	AD = 1.400 p < 0.005	AD = 0.627 p = 0.097	AD = 0.291 p = 0.053	AD = 0.731 p = 0.093	AD = 1.114 p = 0.006	AD = 0.547 p = 0.151	AD = 0.630 p = 0.095
5% PE	8435	49.24	5993	49.25	4009	36.09	**5843**	17.65
5% TL (75%)	8653	51.08	6164	50.97	4235	37.57	5945	17.92
Normal	AD = 0.684 p = 0.070	AD = 0.665 p = 0.078	AD = 0.270 p = 0.663	AD = 0.561 p = 0.139	AD = 0.199 p = 0.880	AD = 0.476 p = 0.229	AD = 0.760 p = 0.045	AD = 0.941 p = 0.016
Mean	11002	72.42	8033	70.47	7218	55.15	6977	27.28
s	1379	12.15	1079	11.37	1837	10.18	618	1.58
5% PE	8228	48.00	5864	47.60	**3524**	34.68	5735	**24.11**
5% TL (75%)	8504	50.42	6080	49.87	3891	36.71	5858	24.42
Non-Parametric								
5% PE	**8735**	**45.22**	**5670**	50.96	3940	34.08	**6164**	**18.25**
5% TL (75%)	8347	44.07	5276	**38.83**	**3460**	**28.87**	6020	17.71

Note: PE = point estimate, TL = tolerance limit, s = standard deviation, AD = Anderson-Darling, p = probability; best fit estimation parameters are displayed in bold.

Ductility is a material's ability to attain high displacement without losing too much strength. For clear wood, the stress distribution in a bending member is related to the compression zone's plasticization. For structural timber-containing defects, this only occurs when the defects are located mainly in the compression zone [57]. The bending test's load-displacement curves (Figure 5) proved that each wood species has a different proportional limit and maximum load. The ductility ratio (μ) of timbers from the experimental results are presented in Table 5. Because the ductility ratio ranges were 2.12–5.32, timber subjected to a bending load may be classified from low to medium ductility according to Eurocode 8 [74]. Agathis had the lowest μ value, which indicates that agathis subjected to bending is the most brittle among other timbers in this study. The agathis specimens were classified as low ductility because their ductility ratio was equal to or less than 4 ($\mu \leq 4$). At the same time, red meranti, mahogany, and pines varied from low to medium ductility. The μ value is thought to affect the beam stability factor (C_L), as the μ is inversely related to E/S_R. In this study, agathis had the highest E/S_R value (Table 3). Ishiguri et al. [73] previously reported that agathis had a high modulus of elasticity (E) and a low modulus of rupture (S_R) value.

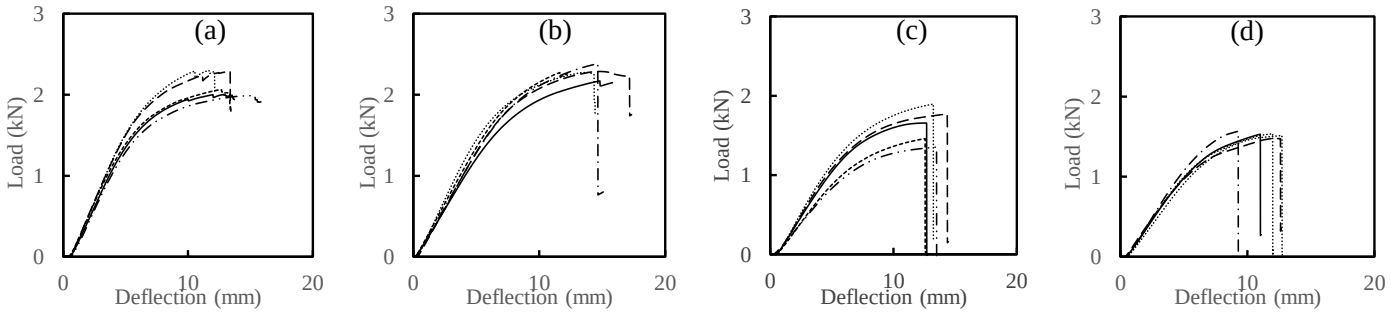


Figure 5. The bending test load–displacement curve: (**a**) red meranti, (**b**) mahogany, (**c**) pine, and (**d**) agathis. (Note: each graph consists of five specimens which were selected randomly from 50 specimens).

Table 5. The small timber beams' ductility ratio (μ).

	N	Min	Max	Mean	*S*	CV (%)
Red meranti	50	2.2	5.0	3.6	0.6	17.9
Mahogany	50	2.3	5.0	3.4	0.6	17.3
Pine	50	2.1	5.3	3.6	0.6	16.7
Agathis	50	2.6	4.0	3.3	0.3	10.1

Note: $\mu \leq 4$ = low ductility, $4 \leq \mu \leq 6$ = medium ductility, $\mu \geq 6$ = high ductility (Eurocode 8 [74]).

3.3. Strength Ratio of the Full-Size Specimens

Wood, as a natural material, has imperfections and defects, which may reduce its strength. The presence of knots [75], the slope of the grain [76], and shakes, checks, and splits can all reduce the E and S_R of timber. Imperfections and defects in wood are often used to determine the wood quality class using visual grading. Visual grading is conducted by converting wood imperfections and defects into a strength ratio (S) to be applied to adjust the strength of a wooden member [77]. S is the ratio of wood strength with defects on its surface to the clear specimen wood strength, and is expressed as a percentage (%) [78]. The S value of the full-size specimens in this study is presented in Table 6. Red meranti had the highest S value, followed by mahogany and pine, while the lowest S value belonged to agathis. A higher S value indicates that the wood has fewer defects.

Table 6. The full-size specimens' strength ratio (S).

Timber Species	Properties	*N*	Min	Max	Mean	*S*	CV (%)
Red meranti	S due to slope of grain (%)	18	40.00	84.50	60.62	14.85	24.49
	S due to knots (%)	18	49.00	100.00	87.58	14.77	16.87
	S due to shakes, checks, splits (%)	18	50.00	100.00	94.44	16.17	17.12
	S total value (%)	18	16.80	84.50	50.27	17.56	34.94
Mahogany	S due to slope of grain (%)	18	40.00	100.00	67.01	16.98	25.33
	S due to knots (%)	18	62.00	100.00	73.36	10.34	14.09
	S due to shakes, checks, splits (%)	18	62.50	100.00	77.96	11.27	14.45
	S total value (%)	18	25.58	74.57	50.03	16.87	33.72
Pine	S due to slope of grain (%)	18	40.00	92.50	68.26	12.29	18.00
	S due to knots (%)	18	73.67	96.25	88.71	7.50	8.45
	S due to shakes, checks, splits (%)	18	50.00	100.00	83.33	24.25	29.10
	S total value (%)	18	14.74	75.50	44.74	18.75	41.91
Agathis	S due to slope of grain (%)	18	40.00	45.98	40.40	1.42	3.53
	S due to knots (%)	18	37.83	100.00	56.89	18.17	31.95
	S due to shakes, checks, splits (%)	18	100.00	100.00	100.00	0.00	0.00
	S total value (%)	18	15.13	40.00	23.03	7.56	32.80

Red meranti and mahogany, which are hardwoods, have a few small knots and their grain direction is relatively straight, however, they have many shakes, checks, and splits. Pine and agathis, which are softwoods, have many knots with large diameter, and the slope of the grain direction means that the S value is low. Each timber species has a different defect variation. The difference in S values is influenced by the wood-working process as well [77]. The process by which logs are converted to sawn lumber affects the slope of the grain. In addition, cutting wood affects the variations in the grain direction. In this study, each specimen's grain direction varied. Distortions of grain direction occur around knots as well, causing large variations in the wood's mechanical properties. The knots and the slope of the grain are factors that significantly affect the S value, especially the slope of grain through the knots. The knots and the slope of the grain have an inverse relationship to wood strength. Timber boards with a 1 in 10 slope of the grain have a 24% lower strength than straight-grained wood [76]. The E value of wood with knots is lower

than the E value of wood without knots [79]. Knot size has a negative correlation with the modulus of elasticity (E) and the modulus of rupture (S_R) [80].

3.4. Flexural Properties of the Full-Size Specimens in Various Loading Configurations

Six loading configurations were programmed in the full-size bending test. Both supports were 38 mm diameter rollers. The modulus of elasticity (E) and modulus of rupture (S_R) value of full-size specimens resulting from the experimental study are shown in Figure 6. Red meranti had the highest E and S_R values, followed by mahogany, pine, and agathis. Red meranti and mahogany, which are hardwoods, have higher E and S_R values than pine and agathis (softwood).

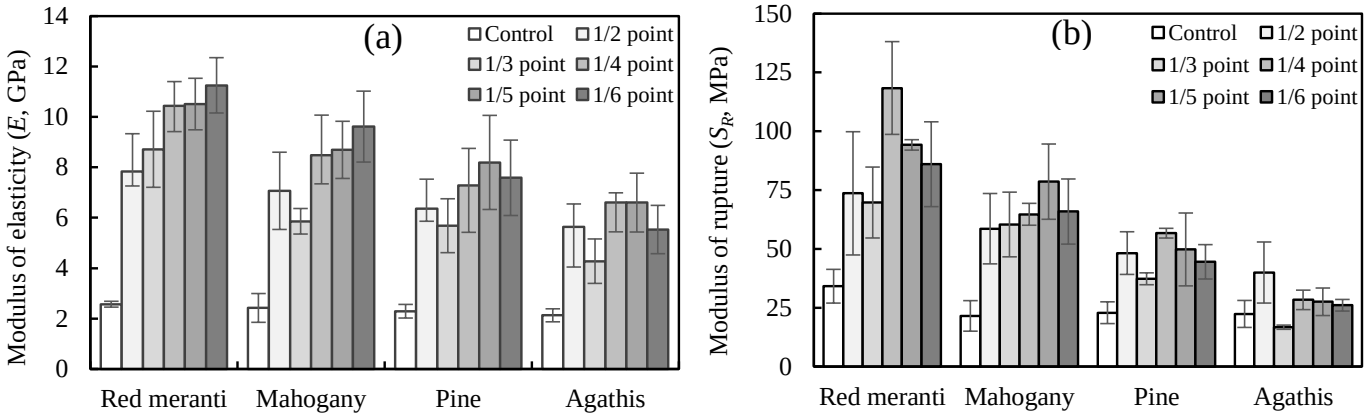


Figure 6. Flexural properties (**a**) modulus of elasticity (E) and (**b**) modulus of rupture (S_R) of full-size specimens subjected to various concentrated loads (Note: control = center-point loading without lateral support; 1/2 point = center-point with lateral support; 1/3 point = third point with lateral support; 1/4 point = fourth point with lateral support; 1/5 point = fifth point with lateral support; 1/6 point = sixth point with lateral support).

When more loading points are applied, the measured values of E and S_R are higher because when the load is spread more evenly, the load received by the beam is more widely distributed, meaning that the beam can withstand a higher load. In the center-point loading configuration, the beam receives all loads from one source; thus, it reaches its critical load and failure more quickly. These results strengthen the findings of Brancheriau et al. [81], who reported that the timber beam in the third point loading configuration produced an E value 19% higher than center-point loading. This shows that more points of loading applied to the bending test lead to higher the E and S_R values.

3.5. Beam Stability Factor (C_L)

The small specimens' beam slenderness ratio (R_B) ranged from 4.4 to 5.6, while for the full-size specimens it ranged from 4.5 to 11.1. The full-size specimens with applied center-point loading without lateral support were categorized as intermediate beams (R_B = 10.6–11.1) in this study, while the other specimens with a slenderness ratio less than 10 ($R_B \leq 10$) were categorized as short beams. The R_B value was affected by the specimen size, irrespective of the loading configuration and lateral support. When more points of loading and lateral supports are applied, the unsupported length (l_u) is shorter, and thus the R_B value is lower.

The ratio between the modulus of elasticity and the modulus of rupture (E/S_R) is necessary to calculate the C_L value. The E/S_R value is an inherent property of wood species; it is assumed to be constant, as the modulus of elasticity (E) is significantly correlated with the modulus of rupture (S_R) (e.g., eucalyptus wood [82], teak and ebony timber [83], tropical timber [8], Guadua bamboo [12], *Gigantochloa apus* bamboo [29,30]). Because E is strongly correlated with the modulus of rupture (S_R), E is a common indicating predictor for strength grading [8,84]. The average E/S_R values of small clear specimens of red

meranti, mahogany, pine, and agathis in this study were 152, 114, 131, and 336, respectively (Table 3). This E/S_R was applied for calculating the C_L value of both small and full-size specimens. The higher the E/S_R, the higher the C_L value, meaning that the beam can more stably resist lateral–torsional buckling. The $C_{L,e}$ values of the small specimens of red meranti, mahogany, pine, and agathis obtained in this study ranged from 0.61–1.25, 0.55–1.35, 0.60–1.39, and 0.85–1.31, respectively, while those of the full-size specimens ranged from 0.41–1.32, 0.22–1.36, 0.32–1.22, and 0.77–1.22, respectively. The variation of the $C_{L,e}$ value is affected by the beam slenderness ratio (R_B) and the ratio of the modulus of elasticity to the modulus of rupture (E/S_R).

The parameter estimations of non-linear regression analysis under Equation (17) are presented in Table 7, and the best-fit formula is Equation (18). The estimated Euler buckling coefficient (K_{bE}) value obtained in this study was 0.413, with 5% lower and 5% upper values of 0.338 and 0.488. These values were not significantly different from the K_{bE} value proposed by Zahn (K_{bE} = 0.438) [41]. The $C_{L,e}$ value of this experimental study was curve fitted using non-linear estimation (Figure 7). Zahn's C_L curve [41] almost coincides with the estimated empirical C_L curve obtained in this study, and is between the 5% lower and 5% upper estimation value of K_{bE}.

$$C_L = \frac{\left[1 + 0.413\frac{E}{S_R {R_B}^2}\right]}{1.9} - \sqrt{\left[\frac{1 + 0.413\frac{E}{S_R {R_B}^2}}{1.9}\right]^2 - \frac{0.413\frac{E}{S_R {R_B}^2}}{0.95}}, \; R^2 = 32.90\% \quad (18)$$

Table 7. Parameter estimation of the Euler buckling coefficient (K_{bE}).

Parameter	Estimate	Standard Error	*t*-Value	*p*-Value	Lower Confident Limit	Upper Confident Limit
$a \cong K_{bE}$	0.413	0.038	10.852	0.00	0.338	0.488

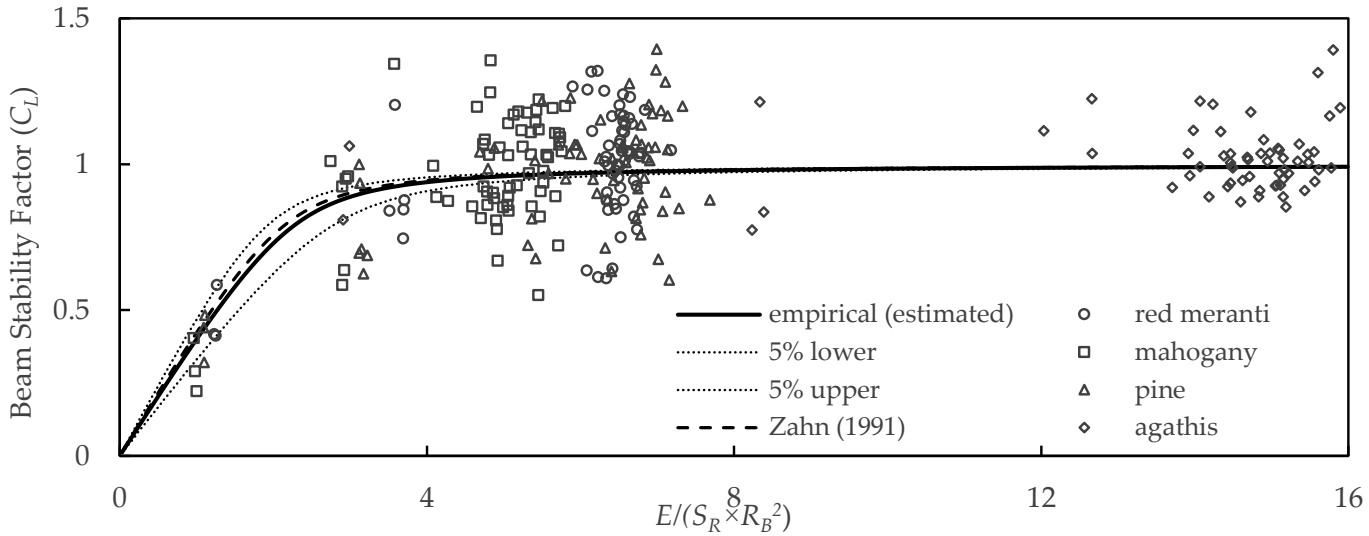


Figure 7. Nonlinear estimation of the empirical beam stability factor ($C_{L,e}$) curve compared to Zahn's C_L curve [41] (Note: Modulus of elasticity (E) and modulus of rupture (S_R) on abscissa were obtained from the average value of the small specimen bending tests).

Multiplying K_{bE} by the factor of 2.74 results in the adjusted Euler buckling coefficient (K_{bE}'), for which the value found in this study was 1.13. The obtained K_{bE}' in this study was similar to that of the NDS (K_{bE}' = 1.20) [35]. The 5% lower and 5% upper values of K_{bE}' were 0.92 and 1.33, respectively, which includes the K_{bE}' value proposed by the NDS. Because the empirical K_{bE}' is similar to that of the NDS, this experimental study approves the NDS C_L equation, and we therefore propose to continue using it. The NDS C_L equation

adopted by SNI 7973:2013 [33] proves reliable for adjusting the reference bending strength of red meranti, mahogany, pines, and agathis sawn lumber.

The obtained $K_{bE}{}'$ values differ among wood species because of the variation of E/S_R; thus, the estimated C_L formula on all R_B ranges from this experiment can be inferred (Figure 8) for each timber species, then compared to the NDS formula. The C_L curve positions of red meranti, mahogany, and pine were below that of the NDS, while the C_L curve of agathis was above it. Agathis has the highest C_L value among the other timbers. The parameter that mostly affects C_L value is E/S_R. The E/S_R value of agathis is the highest due to its low modulus of rupture (S_R) value (Table 3). The order of the C_L curve positions (Figure 8) proportionally corresponds to the E/S_R values. A higher E/S_R value means that the C_L curve will be in the upper position. The C_L value curve of agathis was the highest among the others because the agathis beam did not twist during the bending test; it failed before twisting could occur, indicating inelastic material failure. While red meranti, mahogany, and pine twisted when applying the edgewise mid-point loading bending test, failure occurred when twisting caused the specimen to turn flatwise or slip from the supports, indicating elastic lateral buckling failure. Inelastic failure of the beam happened with small deformation, while elastic member failure was indicated by the long deformation. The deformation value at the yield load is related to the ductility.

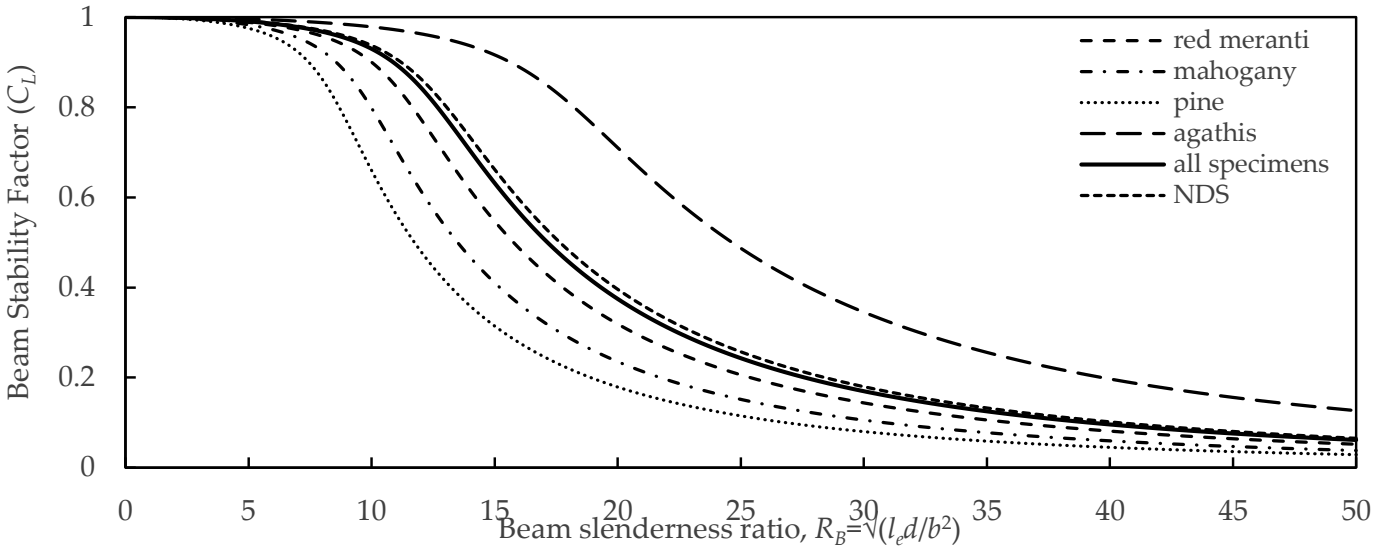


Figure 8. The experimental beam stability factor (C_L) curve applicable to all slenderness ratios (R_B) of each timber species and all specimens as compared to the NDS's curve.

The strength ratio (S) is thought to affect the beam stability factor. The variability of wood mechanical properties is increased in structural timber members due to defects and imperfections (e.g., knots, the slope of the grain, and shakes, checks, and splits) [85]. Agathis contains the most defects among the others, and as such its S value is the lowest. If ascendingly sorted according to their S value, agathis was the lowest, followed by pine, mahogany, and red meranti (Table 5). The order of the S value was inversely proportional to the C_L curve position because it is negatively correlated with E/S_R (Figure 9a). A lower S value indicates that wood has many defects, in which case the C_L curve lies at the upper position. Pelletier and Doudak [86] investigated the lateral–torsional buckling of wood I-joists to account for the effect of the actual end condition and initial imperfection of a beam, and reported that the initial imperfection influences the nonlinear behavior.

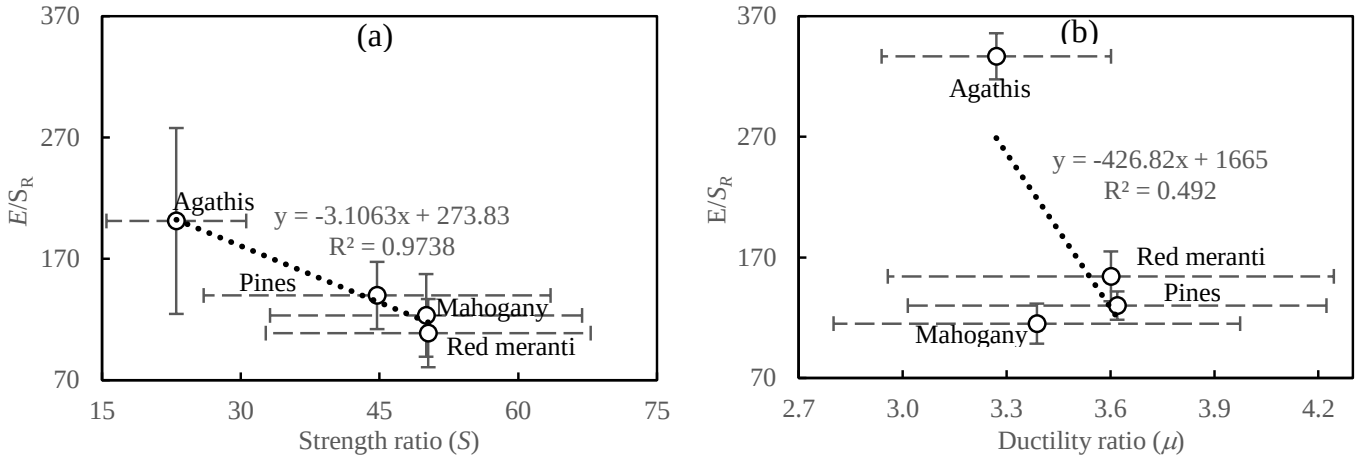


Figure 9. Correlation between the strength ratio (S) and E/S_R of the small specimen (**a**) and between the ductility ratio (μ) and E/S_R of the full-size specimen (**b**). Both strength ratio (S) and ductility ratio (μ) are negatively correlated with E/S_R.

Jorrissen and Fragiacomo [57] reported that wooden tension members, most bending members, and most connections are brittle; columns (buckling) and certain connections are semi-ductile, while compression (both parallel and perpendicular to the grain), connection controlled by embedment, and/or steel failure can be categorized as ductile. In this study, the specimens subjected to a mid-point loading test without lateral support (the intermediate beams) mostly experienced twisting before reaching their failure points. Several agathis intermediate beams did not twist until failure. Agathis subjected to bending moment is the most brittle among others, as its ductility ratio (μ) value is the smallest. The failures of the full-size specimens of agathis occurred before twisting, and only a small deformation occurred before failure; thus, agathis subjected to bending can be categorized as brittle. The maximum load of red meranti, mahogany, and pine occurred when they began to twist. The applied load of red meranti, mahogany, and pine decreased as twisting occurred, and the failure load was much lower than the ultimate load. The beams of red meranti, mahogany, and pine can be categorized as low to medium ductile according to Eurocode 8 [74]. The correlation value between μ and E/S_R is statistically significant ($r = -0.701$). Because the ductility value (μ) (Table 5) has a significant inverse correlation to the E/S_R value (Figure 9b), it is inversely correlated to the C_L value as well. A brittle beam has a higher C_L value than a ductile beam. A brittle beam produces only a small deformation, and inelastic failure happens before beam twisting. In contrast, a ductile beam produces significantly larger deformation, and elastic failure commonly occurs.

3.6. Beam Stability Factor (C_L) Application in Beam Design

Hayatunnufus reported bending tests of timber short beams with a slenderness ratio of 7.40–7.66, resulted in no twisting [87]. The beam stability factor (C_L) is the adjustment factor used to consider the effect of lateral–torsional buckling in intermediate and long beams. C_L is applied as a reducing factor for the allowable bending stress (F_b) in combination with the safety factor, load duration factor (C_D), wet service factor (C_M), temperature (C_t), size factor (C_F), flat use factor (C_{fu}), incising factor (C_i), and repetitive member factor (C_r). The characteristic strength is the 5% exclusion limit ($R_{0.05}$) value from the experimental result. The result of the $R_{0.05}$ value of MOR multiplied by C_L is presented in Figure 10. As shown in Figure 10, less than 5% of specimens lie below the characteristic strength curve multiplied by C_L ($R_{0.05} \times C_L$) (e.g., three red meranti specimens, two mahogany specimens, a pine specimen, and an agathis specimen. Because very few data points lie below the curve, the designer can confidently use the C_L value as an adjustment factor for the reference bending design value. The beam stability factor (C_L) formula obtained in this study is similar to

that of NDS. We suggest that designers continue to use the NDS procedures to adjust the reference bending design value in order to safely and reliably design a beam.

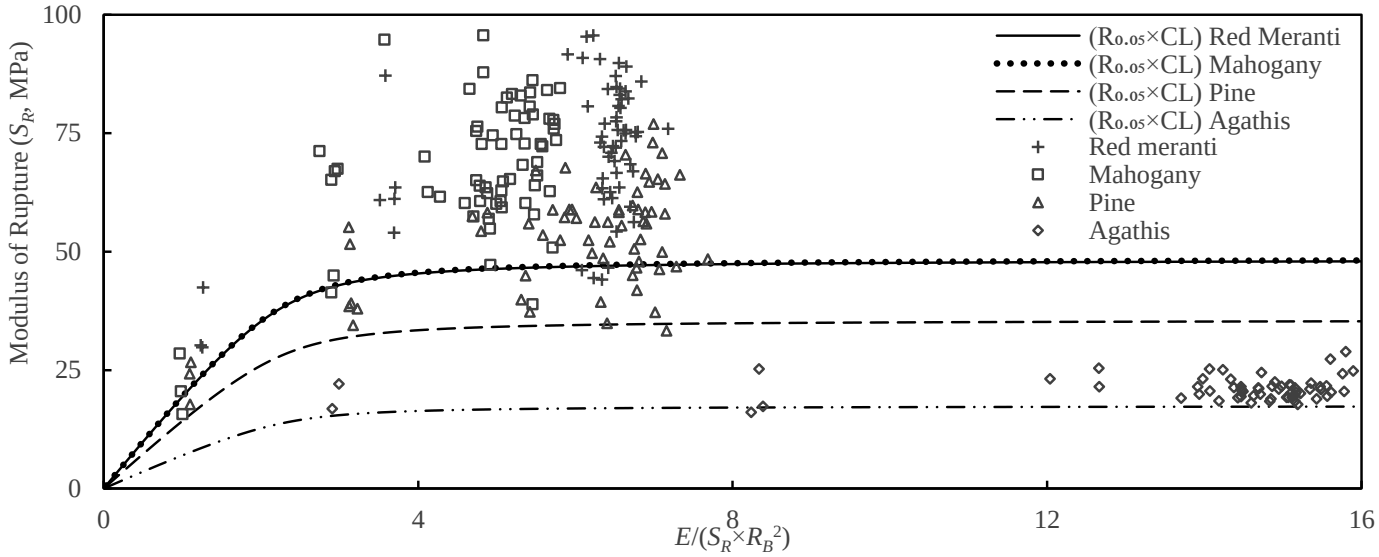


Figure 10. Experimental result of modulus of rupture (S_R) compared to the characteristic strength multiplied by the beam stability factor ($R_{0.05} \times C_L$) (Note: E and S_R on abscissa are the average value of the small-size specimen).

4. Conclusions

The range of sawn lumber beam slenderness ratio in this study was 4.37–11.1, and resulted in an empirical beam stability factor (C_L) ranging widely from 0.32 to 1.39. Curve fitting through nonlinear regression resulted in an estimated Euler buckling coefficient (K_{bE}) value of 0.413. By multiplying the factor of 2.74 by K_{bE}, the adjusted $K_{bE}{}'$ value obtained in this study was 1.13, with the 5% lower and 5% upper values of 0.92 and 1.33, respectively, which agrees with that of the NDS ($K_{bE}{}'$ = 1.20). Because agathis has the lowest ductility (μ), most natural defects (smallest strength ratio, S), and highest E/S_R ratio among others, the agathis beam did not undergo twisting during the bending test; rather, it failed before twisting could occur, indicating inelastic material failure. Meanwhile the other specimens (pinus, mahogany, and red meranti), which have a smaller E/S_R ratio, higher ductility, and fewer natural defects, tended to fail because of their lesser beam stability. This phenomenon resulted in the C_L curve of agathis being the highest among others. The C_L value mathematically relates to the beam slenderness ratio (R_B) and the E/S_R ratio. Because the strength ratio (S) and ductility ratio (μ) have significant inverse correlation with the E/S_R ratio, they are inversely correlated with the C_L value. Applying the C_L value to adjust the characteristic bending strength is safe and reliable, as less than 5% of the specimens lay below the characteristic strength curve multiplied by the C_L ($R_{0.05} \times C_L$). This study shows that designers can safely apply the C_L formula to adjust the red meranti, mahogany, pines, and agathis sawn lumber reference bending design values.

Author Contributions: Conceptualization, E.T.B.; Data curation, E.T.B. and R.H.; Formal analysis, E.T.B. and R.H.; Funding acquisition, E.T.B., D.H. and N.N.; Investigation, E.T.B., E.E. and R.H.; Methodology, E.T.B. and R.H.; Project administration, E.T.B., D.H. and N.N.; Resources, E.T.B.; Supervision, E.T.B. and E.E.; Validation, E.T.B. and R.H.; Visualization, E.T.B. and R.H.; Writing—original draft, E.T.B. and R.H.; Writing—review & editing, E.T.B. All authors have read and agreed to the published version of the manuscript.

Funding: This research was funded by Direktorat Jenderal Pendidikan Tinggi, Riset, dan Teknologi-Kementerian Pendidikan, Kebudayaan, Riset, dan Teknologi-Republik Indonesia grant number 2093/IT.3.L1/PT.01.03/P/B/2022.

Institutional Review Board Statement: This study is not involving humans or animals and the ethical approval is not required.

Informed Consent Statement: Not applicable.

Data Availability Statement: The raw and processed data required to reproduce these findings are available for download from http://dx.doi.org/10.17632/t9k5rh4zy4.3 [88] since 8 January 2021.

Acknowledgments: The authors would like to express many thanks to IPB University (Bogor Agricultural University) (ID), the Ministry of Education and Culture (ID), and the Ministry of Research and Technology (ID) for the finance, permit, facilities, and opportunity to conduct this research.

Conflicts of Interest: The authors declare no conflict of interest.

Abbreviations

a	regression coefficient to estimate the K_{bE}
b	specimen width (mm)
c	non-linear parameter for beam = 0.95
C_D	load duration factor
C_F	size factor
C_{fu}	flat use factor
C_i	incising factor
C_k	beam stability factor limit
C_L	beam stability factor
C_{Le}	empirical beam stability factor
C_M	wet service factor
C_r	repetitive member factor
C_t	temperature factor
d	specimen depth (mm)
E	modulus of elasticity (MPa)
E_{min}	5% lower exclusion value of modulus elasticity (MPa)
F_b	reference bending design value (MPa)
$F_b{}'$	adjusted reference bending design value
F_{bE}	critical buckling design (MPa)
F_u	ultimate load (N)
G_b	specific gravity
K_{bE}	Euler buckling coefficient
$K_{bE}{}'$	adjusted Euler buckling coefficient
L	specimen length (mm)
l_e	effective span length (mm)
l_u	unsupported length (mm)
m_0	mass before the bending test (g)
m_1	mass after the bending test (g)
M_c	moisture content (%)
m_{ot}	mass after oven-drying (g)
$R_{0.05}$	5% exclusion limit value
R_B	beam slenderness ratio
R_k	characteristic value (MPa)
S	strength ratio (%)
S_R	modulus of rupture (MPa)
Greek symbol	
μ	ductility ratio
Δ_u	ultimate displacement (mm)
Δ_y	yield displacement (mm)
ρ	density (g/cm^3)

References

1. Lattke, F.; Lehmann, S. Multi-Storey Residential Timber Construction: Current Developments in Europe. *J. Green Build.* **2007**, *2*, 119–129. [CrossRef]
2. Buchanan, A.; Deam, B.; Pampanin, S.; Fragiacomo, M.; Palermo, A. Multi-Storey Prestressed Timber Buildings in New Zealand. *Struct. Eng. Int. J. Int. Assoc. Bridg. Struct. Eng.* **2008**, *18*, 166–173. [CrossRef]
3. Bahtiar, E.T.; Nugroho, N.; Hermawan, D.; Wirawan, W. Triangle bracing system to reduce the vibration level of cooling tower—Case study in PT Star Energy Geothermal (Wayang Windu) Ltd—Indonesia. *Case Stud. Constr. Mater.* **2018**, *8*, 248–257. [CrossRef]
4. Bahtiar, E.T.; Nugroho, N.; Rahman, M.M.; Arinana; Sari, R.K.; Wirawan, W.; Hermawan, D. Estimation the remaining service-lifetime of wooden structure of geothermal cooling tower. *Case Stud. Constr. Mater.* **2017**, *6*, 91–102. [CrossRef]
5. Bahtiar, E.T.; Nugroho, N.; Arinana, D.A. Pendugaan Sisa Umur Pakai Kayu Komponen Cooling Tower di Pembangkit Listrik Tenaga Panas Bumi (PLTP) Unit II Kamojang (Estimating the Remaining Life of Wood Cooling Tower Component in Geothermal Power Plant Unit II Kamojang). *J. Tek. Sipil.* **2012**, *19*, 103–113. [CrossRef]
6. Lamar, D.M.; Schafer, B.W. Structural Analyses of Two Historic Covered Wooden Bridges. *J. Bridg. Eng.* **2004**, *9*, 623–633. [CrossRef]
7. Firmanti, A.; Komatsu, K.; Kawai, S. Effective Utilization of Fast-Growing Acacia mangium Willd. Timber As a Structural Material. *J. Trop. Wood Sci. Technol.* **2007**, *5*, 29–37.
8. Firmanti, A.; Bachtiar, E.T.; Surjokusumo, S.; Komatsu, K.; Kawai, S. Mechanical stress grading of tropical timbers without regard to species. *J. Wood Sci.* **2005**, *51*, 339–347. [CrossRef]
9. Steffen, A.; Johansson, C.-J.; Wormuth, E.-W. Study of the relationship between flatwise and edgewise modull of elasticity of sawn timber as a means to improve mechanical strength grading technology. *Holz als Roh-Werkst.* **1997**, *55*, 245–253. [CrossRef]
10. Oscarsson, J.; Olsson, A.; Enquist, B. Optimization of machine strength grading of structural timber by means of bending MOE profiles with high resolution. In Proceedings of the 18th International Nondestructive Testing and Evaluation of Wood Symposium, Madison, WI, USA, 24−27 September 2013.
11. Bodig, J.; Jayne, B. *Mechanics of Wood and Wood Composites*; Van Nostrand Reinhold Company: New York, NY, USA, 1982.
12. Bahtiar, E.T.; Malkowska, D.; Trujillo, D.; Nugroho, N. Experimental study on buckling resistance of *Guadua angustifolia* bamboo column. *Eng. Struct.* **2020**, *228*, 111548. [CrossRef]
13. Nugroho, N.; Bahtiar, E.T. Buckling formulas for designing a column with *Gigantochloa apus*. *Case Stud. Constr. Mater.* **2021**, *14*, e00516. [CrossRef]
14. Bahtiar, E.T.; Imanullah, A.P.; Hermawan, D.; Nugroho, N. Structural grading of three sympodial bamboo culms (Hitam, Andong, and Tali) subjected to axial compressive load. *Eng. Struct.* **2018**, *181*, 233–245. [CrossRef]
15. Bahtiar, E.T.; Trujillo, D.; Nugroho, N. Compression resistance of short members as the basis for structural grading of Guadua angustifolia. *Constr. Build. Mater.* **2020**, *249*, 118759. [CrossRef]
16. American Wood Council. *1997 NDS Commentary*; American Wood Council: Leesburg, VA, USA, 1997.
17. Pi, Y.-L.; Bradford, M.A. Thermoelastic lateral-torsional buckling of fixed slender beams under linear temperature gradient. *Int. J. Mech. Sci.* **2008**, *50*, 1183–1193. [CrossRef]
18. Hindman, D.P.; Manbeck, H.B.; Janowiak, J.J. Measurement and prediction of lateral torsional buckling loads of composite wood materials: Rectangular sections. *For. Prod. J.* **2005**, *55*, 42.
19. Hassan, O.A.; Johansson, C. Glued laminated timber and steel beams. *J. Eng. Des. Technol.* **2018**, *16*, 398–417. [CrossRef]
20. *ASTM D143*; Standard Test Methods for Small Clear Specimens of Timber. ASTM: West Conshohocken, PA, USA, 2002.
21. Jamil, A.M.; Zamin, J.M.; Omar, M.M. Relationship between mechanical properties of structural size and small clear specimens of timber. *J. Trop. For. Sci.* **2013**, *25*, 12–21.
22. Bahtiar, E.T.; Nugroho, N.; Nandika, D. Daily Cycle of Air Temperature and Relative Humidity Effect to Creep Deflection of Wood Component of Low-cost House in Cibeureum-Bogor, West Java, Indonesia. *Asian J. Sci. Res.* **2014**, *7*, 501–512. [CrossRef]
23. Bahtiar, E.T.; Nugroho, N.; Surjokusumo, S. Estimating Young's Modulus and Modulus of Rupture of Coconut Logs using Reconstruction Method. *Civ. Eng. Dimens.* **2010**, *12*, 65–72. [CrossRef]
24. *BS 373:1957*; Methods of Testing Small Clear Specimens of Timber. British Standards: London, UK, 1957.
25. Bahtiar, E.T.; Nugroho, N.; Karlinasari, L.; Darwis, A.; Surjokusumo, S. Rasio Ikatan Pembuluh sebagai Substitusi Rasio Modulus Elastisitas pada Analisa Layer System pada Bilah Bambu dan Bambu Laminasi. *J. Tek. Sipil* **2014**, *21*, 147. [CrossRef]
26. Veldman, S.; Bergsma, O.; Beukers, A. Bending of anisotropic inflated cylindrical beams. *Thin-Walled Struct.* **2005**, *43*, 461–475. [CrossRef]
27. Manikandan, P.; Rao, G.S.; Srinath, J.; Sharma, V.; Narayanan, P.R.; Sharma, S.; George, K.M. Axial and Bending Fatigue Testing of AISI 304 L Plumbing Tubes Used for Launch Vehicles Control System. *Mater. Sci. Forum* **2015**, *830–831*, 187–190. [CrossRef]
28. Trujillo, D.; Jangra, S.; Gibson, J.M. Flexural properties as a basis for bamboo strength grading. *Proc. Inst. Civ. Eng.—Struct. Build* **2017**, *170*, 284–294. [CrossRef]
29. Nurmadina; Nugroho, N.; Bahtiar, E.T. Structural grading of *Gigantochloa apus* bamboo based on its flexural properties. *Constr. Build. Mater.* **2017**, *157*, 1173–1189. [CrossRef]
30. Nugroho, N.; Bahtiar, E.T. Grading Development of Indonesian Bamboo Culm: Case Study on Tali Bamboo (*Gigantochloa apus*). In Proceedings of the 2018 World Conference on Timber Engineering, Seoul, Korea, 20 August 2018.
31. Saoula, A.; Meftah, S.A.; Mohri, F.; Daya, E.M. Lateral buckling of box beam elements under combined axial and bending loads. *J. Constr. Steel Res.* **2016**, *116*, 141–155. [CrossRef]
32. Galambos, T.V.; Surovek, A.E. *Structural Stability of Steel*; John Wiley & Sons, Inc.: Hoboken, NJ, USA, 2008.

33. *SNI 7973:2013*; Spesifikasi Desain Untuk Konstruksi Kayu. Badan Standardisasi Nasional: Jakarta, Indonesia, 2013.
34. Suryoatmono, B.; Tjondro, A. Lateral-torsional buckling of orthotropic rectangular section beams. In Proceedings of the 10th World Conference on Timber Engineering, Miyazaki, Japan, 2–5 June 2008.
35. American National Standard Institution; American Wood Council. *NDS, National Design Specification for Wood Construction, ASD/LRFD*; American National Standard Institution: Washington, DC, USA, 2012.
36. *EN 1995-1-1:2004*; Eurocode 5: Design of Timber Structures—Part 1-1: General—Common Rules and Rules for Buildings. The European Union: Brussels, Belgium, 2004.
37. Zahn, J.J. Design of Wood Members Under Combined Load. *J. Struct. Eng.* **1986**, *112*, 2109–2126. [CrossRef]
38. American Wood Council. *National Design Specification (NDS) for Wood Construction*; American Wood Council: Leesburg, VA, USA, 1986.
39. Zahn, J. Combined-load Stability Criterion for wood-beam columns. *J. Struct. Eng.* **1988**, *114*, 22981. [CrossRef]
40. American Forest and Paper Association. *ANSI/NFoPA NDS-1991 National Design Specification for Wood Construction*; American Forest and Paper Association: Washington, DC, USA, 1991.
41. Zahn, J.J. Biaxial Beam-Column equation for Wood Members. In Proceedings of the 9th structures Congress Proceedings, New York, NY, USA, 29 April–1 May 1991; pp. 56–59.
42. Kimble, R.E.; Bender, D.A. Stability of Built-Up Timber Beams and Columns: Accounting for Modulus of Elasticity Variability. *Pr. Period. Struct. Des. Constr.* **2010**, *15*, 272–277. [CrossRef]
43. Du, Y.; Mohareb, M.; Doudak, G. Nonsway Model for Lateral Torsional Buckling of Wooden Beams under Wind Uplift. *J. Eng. Mech.* **2016**, *142*, 04016104. [CrossRef]
44. Du, Y.; Mohareb, M.; Doudak, G.; Du, B.Y. Sway Model for the Lateral Torsional Buckling Analysis of Wooden Twin-beam-deck Systems. *Structures* **2019**, *19*, 19–29. [CrossRef]
45. Hu, Y.; Mohareb, M.; Doudak, G. Lateral Torsional Buckling of Wooden Beams with Midspan Lateral Bracing Offset from Section Midheight. *J. Eng. Mech.* **2017**, *143*, 04017134. [CrossRef]
46. Hu, Y.; Mohareb, M.; Doudak, G. Effect of Eccentric Lateral Bracing Stiffness on Lateral Torsional Buckling Resistance of Wooden Beams. *Int. J. Struct. Stab. Dyn.* **2018**, *18*, 1850027. [CrossRef]
47. St-Amour, R.; Doudak, G. Experimental and numerical investigation of lateral torsional buckling of wood I-joists. *Can. J. Civ. Eng.* **2018**, *45*, 41–50. [CrossRef]
48. Burow, J.R.; Manbeck, H.B.; Janowiak, J.J. Lateral Stability Considerations for Composite Wood I-Joists. In Proceedings of the ASAE Annual International Meeting, Tampa, FL, USA, 17–20 July 2005.
49. Sahraei, A.; Pezeshky, P.; Mohareb, M.; Doudak, G. Simplified expressions for elastic lateral torsional buckling of wooden beams. *Eng. Struct.* **2018**, *174*, 229–241. [CrossRef]
50. Xiao, Q.; Doudak, G.; Mohareb, M. Numerical and experimental investigation of lateral torsional buckling of wood beams. *Eng. Struct.* **2017**, *151*, 85–92. [CrossRef]
51. Balaz, I. Lateral Torsional Buckling of Timber Beams. *Wood Res.* **2005**, *50*, 51–58.
52. *AFPA-TR14*; Designing for Lateral-Torsional Stability in Wood Members. American Wood Council: Washington DC, USA, 2003.
53. *ASTM D2915*; Standard Practice for Evaluating Allowable Properties for Grades of Structural Lumber. ASTM: West Conshohocken, PA, USA, 2002. [CrossRef]
54. *ASTM D5457*; Standard specification for computing reference resistance of wood based materials and structural connections for load and resistance factor design. ASTM: West Conshohocken, PA, USA, 2002.
55. Blaß, H.J.; Schädle, P. Ductility aspects of reinforced and non-reinforced timber joints. *Eng. Struct.* **2011**, *33*, 3018–3026. [CrossRef]
56. Muñoz, W.; Salenikovich, A.; Mohammad, M.; Quenneville, P. Determination of yield point and ductility of timber assemblies: In search for a harmonised approach. In Proceedings of the 10th World Conference on Timber Engineering, Miyazaki, Japan, 2–5 June 2008.
57. Jorissen, A.; Fragiacomo, M. General notes on ductility in timber structures. *Eng. Struct.* **2011**, *33*, 2987–2997. [CrossRef]
58. Karacabeyli, E.; Ceccotti, A. Nailed Wood-Frame Shear Walls for Seismic Loads: Test Results and Design Considerations. In *Structural Engineering World Wide*; SCIRP: Wuhan, China, 1999; pp. 1–9.
59. Yasumura, M.; Kawai, N. Estimating seismic performance of wood-framed structures. In Proceedings of the 5th World Conference on Timber Engineering, Montreux, Switzerland, 17–20 August 1998; Volume 2, pp. 564–571.
60. Foliente, G.C. Issues in seismic performance testing and evaluation of timber structural systems. In Proceedings of the International Wood Engineering Conference, New Orleans, LA, USA, 28–31 October 1996; p. 8.
61. *EN 12512:2001/A1:2005*; Timber Structures—Test methods—Cyclic Testing of Joints Made with Mechanical Fasteners. European Committee for Standardization: Bruxelles, Belgium, 2005.
62. *SIA 265:2003*; Timber Structures. Swiss Society of Engineers and Architects: Zurich, Switzerland, 2003.
63. Foliente, G.C.; Leicester, R.H. Evaluation of mechanical joint systems in timber structures. In Proceedings of the 25th Forest Products Research Conference, Melbourne, VIC, Australia, 18–21 November 1996; pp. 2–16.
64. *ASTM D245*; Standard Practice for Establishing Structural Grades and Related Allowable Properties for Visually Graded Lumber. ASTM: West Conshohocken, PA, USA, 2000. [CrossRef]
65. Bergou, E.H.; Diouane, Y.; Kungurtsev, V. Convergence and Complexity Analysis of a Levenberg–Marquardt Algorithm for Inverse Problems. *J. Optim. Theory Appl.* **2020**, *185*, 927–944. [CrossRef]
66. Wistara, N.J.; Sukowati, M.; Pamoengkas, P. The properties of red meranti wood (*Shorea leprosula Miq*) from stand with thinning and shade free gap treatments. *J. Indian Acad. Wood Sci.* **2016**, *13*, 21–32. [CrossRef]

67. Alokabel, K.; Lay, Y.E.; Wonlele, T. Penentuan Kelas Kuat Kayu Lokal di Pulau Timor Sebagai Bahan Konstruksi. *JUTEKS J. Tek. Sipil* **2018**, *2*, 139–148. [CrossRef]
68. Lempang, M. Basic properties and uses of agathis (*Agathis hamii* M. Dr.) wood from South Sulawesi. *J. Penelit. Kehutan. Wallacea* **2017**, *6*, 157–167. [CrossRef]
69. *NI-5 PKKI 1961*; Peraturan Konstruksi Kayu Indonesia. PKKI: Jakarta, Indonesia, 1961.
70. Ong, C.B.; Ansell, M.P.; Chang, W.-S.; Walker, P. Bending properties of finger-jointed Malaysian dark red meranti. *Int. Wood Prod. J.* **2019**, *10*, 49–54. [CrossRef]
71. Anoop, E.V.; Jijeesh, C.M.; Sindhumathi, C.R.; Jayasree, C.E. Wood physical, Anatomical and Mechanical properties of Big Leaf Mahogany (*Swietenia macrophylla* Roxb) a potential exotic for South India. *Res. J. Agric. For. Sci.* **2014**, *2*, 7–13.
72. Darmawan, W.; Nandika, D.; Afaf, B.D.H.; Rahayu, I.; Lumongga, D. Radial Variation in Selected Wood Properties of Indonesian Merkusii Pine. *J. Korean Wood Sci. Technol.* **2018**, *46*, 323–337. [CrossRef]
73. Ishiguri, F.; Wahyudi, I.; Iizuka, K.; Yokota, S.; Yoshizawa, N. Radial Variation of Wood Property in *Agathis* sp. and *Pinus insularis* Growing at Plantation in Indonesia. *Wood Res. J.* **2010**, *1*, 1–6.
74. *Eurocode 8*; Design of structures for earthquake resistance. European Comission: Brussel, Belgium, 2005.
75. Szabolcs, K.; Sandor, F.; Jozsef, A.; Taschner, R. Effect of knots on the bending strength and the modulus of elasticity of wood. *Wood. Res.* **2013**, *58*, 617–626.
76. Pope, D.; Marcroft, J.; Whale, L. The effect of global slope of grain on the bending strength of scaffold boards. *Holz als Roh- Werkst.* **2005**, *63*, 321–326. [CrossRef]
77. Bahtiar, E.T. Keandalan modulus of elasticity (MOE) untuk menduga kekuatan kayu bercacat akibat lubang bor. *JTHH* **2005**, *18*, 80–90.
78. Mardikanto, T.R.; Karlinasari, L.; Bahtiar, E.T. *Sifat Mekanis Kayu*; IPB Press: Bogor, Indonesia, 2017.
79. Rocha, M.F.V.; Costa, L.R.; Costa, L.J.; De Araújo, A.C.C.; Soares, B.C.D.; Hein, P. Wood Knots Influence the Modulus of Elasticity and Resistance to Compression. *Floresta e Ambient.* **2018**, *25*, e20170906. [CrossRef]
80. Brunetti, M.; Nocetti, M.; Burato, P. Strength Properties of Chestnut Structural Timber with Wane. *Adv. Mater. Res.* **2013**, *778*, 377–384. [CrossRef]
81. Brancheriau, L.; Bailleres, H.; Guitard, D. Comparison between modulus of elasticity values calculated using 3 and 4 point bending tests on wooden samples. *Wood Sci. Technol.* **2002**, *36*, 367–383. [CrossRef]
82. Hein, P.R.G.; Silva, J.; Brancheriau, L. Correlations among microfibril angle, density, modulus of elasticity, modulus of rupture and shrinkage in 6-year-old *Eucalyptus urophylla* × *E. grandis*. *Maderas Cienc Y Tecnol.* **2013**, *15*, 171–182. [CrossRef]
83. Sholadoye, I.O.; Abubakar, I.; Annafi, Q.B.; Ejeh, S.P. Evaluation of Some Wood Properties of Nigeria Timber Using Four-Point Bending Test. *Adv. Multidiscip. Res. J.* **2016**, *2*, 133–144.
84. Divos, F.; Tanaka, T. Lumber Strength Estimation by Multiple Regression. *Holzforschung* **1997**, *51*, 467–471. [CrossRef]
85. Machado, J.S.; Palma, P. Non-destructive evaluation of the bending behaviour of in-service pine timber structural elements. *Mater. Struct.* **2010**, *44*, 901–910. [CrossRef]
86. Pelletier, B.; Doudak, G. Investigation of the lateral-torsional buckling behaviour of engineered wood I-joists with varying end conditions. *Eng. Struct.* **2019**, *187*, 329–340. [CrossRef]
87. Hayatunnufus, A.; Nugroho, N.; Bahtiar, E.T. Faktor Stabilitas Balok Kayu pada Konfigurasi Pembebanan Terpusat. *J. Tek. Sipil dan Lingkung.* **2022**, *7*, 129–146. [CrossRef]
88. Bahtiar, E.T. *Experimental Study on Flexural Buckling of Timber, Mendeley Data V3*; Elsevier Inc.: NY, USA, 2020. [CrossRef]